Proceedings of the ASME 2020
Dynamic Systems and Control Conference
DSCC2020
October 5-7, 2020, Virtual, Online

DSCC2020-3203

NONLINEAR HIERARCHICAL MPC FOR MAXIMIZING AIRCRAFT THERMAL ENDURANCE

Daniel D. Leister
Department of Mechanical Engineering
The University of Texas at Dallas
Richardson, Texas, 75080
Daniel.Leister@UTDallas.edu

Justin P. Koeln*
Department of Mechanical Engineering
The University of Texas at Dallas
Richardson, Texas, 75080
Justin.Koeln@UTDallas.edu

ABSTRACT

In modern high-performance aircraft, the Fuel Thermal Management System (FTMS) plays a critical role in the overall thermal energy management of the aircraft. Actuator and state constraints in the FTMS limit the thermal endurance and capabilities of the aircraft. Thus, an effective control strategy must plan and execute optimized transient fuel mass and temperature trajectories subject to these constraints over the entire course of operation. For the control of linear systems, hierarchical Model Predictive Control (MPC) has shown to be an effective approach to coordinating both short- and long-term system operation with reduced computational complexity. However, for controlling nonlinear systems, common approaches to system linearization may no longer be effective due to the long prediction horizons of upper-level controllers. This paper explores the limitations of using linear models for hierarchical MPC of the nonlinear FTMS found in aircraft. Numerical simulation results show that linearized models work well for lower-level controllers with short prediction horizons but lead to significant reductions in aircraft thermal endurance when used for upper-level controllers with long prediction horizons. Therefore, a mixed-linearity hierarchical MPC formulation is presented with a nonlinear upper-level controller and a linear lower-level controller to achieve both high performance and high computational efficiency.

*Address all correspondence to this author.

1 INTRODUCTION

In using Model Predictive Control (MPC) for the control of nonlinear systems, it is a common practice to linearize system dynamics in order to formulate the MPC optimization problem as either a Linear Program (LP) or a Quadratic Progam (QP) that can be solved quickly online in real-time. While linearization can be implemented in a variety of ways, it is typical for the dynamics to be linearized either once about a desired operating condition or repeatedly about the current operating condition at every update of the MPC controller. Historically, these approaches to linearization have proven effective when the control objective drives the system to a predetermined operating condition (see [1] and the references therein). However, the effectiveness of this linearization approach is unclear when the control objective goes beyond steady-state regulation or reference tracking.

This paper focuses on the role of system nonlinearity in the optimization of high-level system behavior with specific application to aircraft energy management, where the control objective is to maximize thermal endurance. In modern high-performance aircraft, the Fuel Thermal Management System (FTMS) serves the important role of absorbing thermal energy (heat) from other subsystems. Some of this energy is removed from the aircraft via the fuel sent to the engine while the remainder of this energy is stored in the fuel tanks. While the fuel tanks can store a significant amount of thermal energy, due to the considerable mass of fuel in the tanks, the amount of available energy storage is limited by both an upper temperature bound and the monotonically decreasing amount of fuel in the aircraft. Thermal endurance is defined as the length of time an aircraft can operate before

the fuel in the FTMS exceeds these predetermined upper temperature bounds [2]. With the increasing heat loads associated with greater electrification and rising demands for aircraft performance, thermal endurance has become a major factor limiting the capabilities of modern high-performance aircraft [3–5].

As a result, optimizing the operation of the FTMS is critical to maximizing aircraft capability and significant research efforts have focused on modeling and control of a wide variety of FTMS architectures [6–12]. Recently, a dual-tank FTMS has been shown to increase the thermal endurance of an aircraft when compared to a single-tank system with the same amount of fuel [2]. The benefits of a dual-tank FTMS were demonstrated experimentally in [13] using a small-scale experimental system designed using dimensional analysis to achieve dynamic similitude to a full-scale aircraft system. Through detailed analysis of the FTMS dynamics, [2] proves that the thermal endurance achieved by the proposed dual-tank system will exceed that of a single-tank system by strategically controlling the fuel flow from a recirculation tank and a reservoir tank. While the nonlinear dynamics were considered when analyzing the FTMS behavior, a LQR-type controller was developed based on a linearized system model to track a set of predetermined references. These references where chosen offline in an effort to maximize thermal endurance based on steady-state system analysis.

As shown in [2], it is clear that the operation of the FTMS has a significant impact on thermal endurance. Therefore, this paper focuses on optimizing FTMS operation using MPC to directly maximize thermal endurance subject to actuator and state constraints. In particular, this paper demonstrates the need to include the nonlinearities of the FTMS in the MPC prediction model based on the associated reduction in thermal endurance incurred when using linear prediction models. To overcome the computational limits associated with solving Nonlinear Programs (NLPs) online, a mixed-linearity hierarchical MPC formulation is proposed. To reduce computational cost, the upper-level controller is designed with a slow update rate and a nonlinear model of the system to plan long-term state and input trajectories that maximize thermal endurance. The lower-level controller is designed with a fast update rate and linear model of the system to refine the control decision made by the upper-level controller and provide improved disturbance rejection. Waypoint-based coordination is used to guide the lower-level controller based on the desired state trajectory determined by the upper-level controller [14]. Simulation results demonstrate the practicality of this mixed-linearity hierarchical MPC approach and the improved thermal endurance achieved by including system nonlinearities in the prediction horizon.

The remainder of the paper is organized as follows. Section 2 introduces the specific FTMS from [2] used for this study and assesses the modeling error introduced by system linearization. The importance of including system nonlinearities when maximizing thermal endurance is established through open-loop state and input trajectory optimization in Section 3. Details of the closed-loop MPC architectures compared in this work are presented in Section 4. Numerical simulation results in Section 5 demonstrate the value of the proposed mixed-linearity hierarchical MPC formulation for several operating scenarios including both constant and time-varying heat loads. Finally, Section 6 summarizes the conclusions of the paper and provides future research directions.

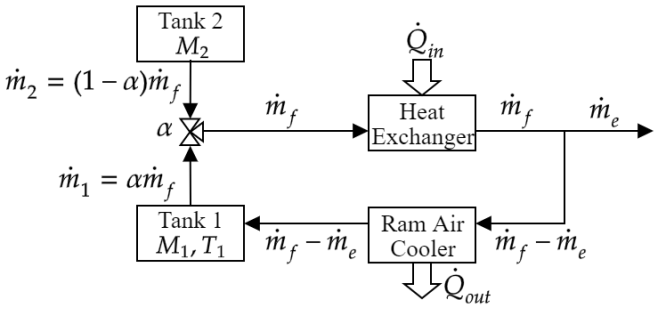

FIGURE 1: Dual-tank FTMS architecture modified from [2].

2 AIRCRAFT FTMS MODEL

2.1 Model Summary

While a number of different FTMS architectures have been studied, each system 1) uses pumped fuel flow to collect thermal energy from various heat sources, 2) removes some of this energy from the aircraft by burning a portion of this heated fuel in the aircraft's engine, and 3) has the ability to cool some of the remaining fuel flow before returning to the fuel tank serving as energy storage. The specific FTMS architecture used in this paper is shown in Fig. 1 and is modeled to have the same dynamic behavior as the dual-tank system from [2]. This system is modeled with three states corresponding to the mass of fuel in the recirculation tank, M_1, the mass of fuel in the reservoir tank, M_2, and the temperature of the fuel in the recirculation tank, T_1. Since fuel can only drain from the reservoir tank, the temperature of fuel in Tank 2, T_2, is assumed constant. Assuming a constant pumped fuel mass flow rate $\dot{m}_f$ and a constant fuel mass flow to the engine, $\dot{m}_e$, the recirculation flow rate that returns to Tank 1 is $\dot{m}_f - \dot{m}_e$. In this simplified system, the only control input is α, which denotes the fraction of pumped fuel coming from Tank 1 such that $\dot{m}_1 = \alpha\dot{m}_f$. As a result, the fuel coming from Tank 2 is $\dot{m}_2 = (1-\alpha)\dot{m}_f$. The pumped fuel is used to absorb heat $\dot{Q}_{in}$ from other subsystems and the fuel returning to Tank 1 passes though a ram air cooler to remove heat $\dot{Q}_{out}$.

From conservation of mass, the differential equations governing the mass of fuel stored in each of the two tanks are

$$\dot{M}_1 = (1-\alpha)\dot{m}_f - \dot{m}_e, \tag{1a}$$

$$\dot{M}_2 = -(1-\alpha)\dot{m}_f. \tag{1b}$$

From conservation of energy, the differential equation governing the temperature of fuel in Tank 1 is

$$\dot{M}_1 c_v T_1 + M_1 c_v \dot{T}_1 = (\dot{m}_f - \dot{m}_e) c_v T_{1,in} - \alpha \dot{m}_f c_v T_1, \quad (2)$$

where c_v is the specific heat of fuel at constant volume and $T_{1,in}$ is the temperature of the fuel exiting the ram air cooler and returning to Tank 1. Neglecting the dynamics of the remainder of the components in Fig. 1, the temperature of the fuel entering Tank 1 is

$$T_{1,in} = T_e - \frac{\dot{Q}_{out}}{(\dot{m}_f - \dot{m}_e) c_v}, \quad (3)$$

where

$$T_e = \alpha T_1 + (1-\alpha) T_2 + \frac{\dot{Q}_{in}}{\dot{m}_f c_v}, \quad (4)$$

is the temperature of the fuel entering the engine. As described in detail in [2], $\dot{Q}_{in}$ is the total heat load from several sources with

$$\dot{Q}_{in} = \dot{Q}_F + \dot{Q}_{h_v} + \dot{Q}_{h_e} + P_p + K_{Q_h} \dot{m}_f, \quad (5)$$

where $\dot{Q}_F$ is the heat from the Full Authority Digital Engine Controller (FADEC), $\dot{Q}_{h_v}$ is the heat from a Vapor Cycle System (VCS), $\dot{Q}_{h_e}$ is the heat from engine lubrication system, and $P_p + K_{Q_h} \dot{m}_f$ is the heat from the fuel pump, assumed to be a linear function of $\dot{m}_f$. Additionally, the heat removed from the system by the ram air cooler is defined in [2] as

$$\dot{Q}_{out} = (\dot{m}_f - \dot{m}_e) c_v (1 - e^{-U})(T_e - T_w), \quad (6)$$

where U is is the number of heat transfer units for the heat exchanger and T_w is the cold side wall temperature. Both U and T_w are assumed constant.

Combining (1)-(6), the overall nonlinear dynamics of the system can be written generically as the control-affine nonlinear system

$$\dot{x} = f(x,d) + g(x,d)u, \quad (7)$$

where $x = [M_1 \; M_2 \; T_1]^\top$ and $u = \alpha$. The disturbance d is taken to be $d = \dot{Q}_{h_v}$ to allow for a time-varying heat load from the VCS, which will be used in Section 5. Table 1 includes the values of the model parameters defined in (1)-(6) based on the values used in [2]. Note that the nonlinearities in the system dynamics are restricted to the dynamics for T_1 and arise from i) the product between the control input α governing the fuel flow rates in the system and the temperature state T_1, which is common in systems with heat transfer due to fluid flow, and ii) the division by the mass of fuel M_1, which is common for any system governed by conservation of energy with time-varying thermal capacitance.

TABLE 1: SYSTEM PARAMETERS.

Variable	Description	Units	Nominal Value[a]	Lower Bound	Upper Bound
M_1	Recirculation tank mass	kg	200	30	2850
M_2	Reservoir tank mass	kg	2850	0	2850
T_1	Recirculation fuel temperature	K	288	280	333
T_2	Reservoir fuel temperature	K	288	-	-
$\dot{m}_f$	Pumped fuel flow rate	kg	1.0	-	-
$\dot{m}_e$	Engine fuel flow rate	kg	0.26	-	-
α	Recirculation fuel fraction	-	-	0	1.0
c_v	Fuel specific heat	J/(kg·K)	2,010	-	-
$\dot{Q}_F$	FADEC heat input	W	1,000	-	-
$\dot{Q}_{h_v}$	VCS heat input	W	55,000	-	-
$\dot{Q}_{h_e}$	Engine heat input	W	10,000	-	-
P_p	Fuel pump power	W	50,000	-	-
K_{Q_h}	Fuel pump heat input coeff.	W/kg	-6,618	-	-
U	Heat Transfer Units	-	-0.37	-	-
T_w	Heat exchanger cold wall temperature	K	238	-	-

[a] Also serves as the initial value for system states M_1, M_2, and T_1.

2.2 Discretization and Linearization

For implementing discrete-time optimization and MPC, the nonlinear continuous-time dynamics from (7) must be discretized. This paper employs a forward Euler discretization where, for a discrete time step size of Δt, the state derivative is approximated as $\dot{x} \approx \frac{x_{k+1} - x_k}{\Delta t}$, with k indexing the discrete time steps. Thus the discrete-time approximation of (7) is

$$x_{k+1} = x_k + \Delta t \left[f(x_k, d_k) + g(x_k, d_k) u_k \right]. \quad (8)$$

While an optimization problem based on (8) would result in a NLP, the continuous-time dynamics from (7) can be linearized and then discretized in order to benefit from the reduced computational burden associated with solving a LP or QP, depending on the cost function design. For linearization, this paper employs a Taylor series approximation of $f(x,d)$ and $g(x,d)u$ about nominal operating conditions x^o, d^o, and u^o. Note that these nominal operating conditions do not need to be an equilibrium of (7), which is important considering the monotonically decreasing amount of fuel stored in the fuel tanks. From this Taylor series approximation, the discrete-time linear approximation of (7) is

$$x_{k+1} = A^o x_k + B^o u_k + W^o d_k, \quad (9)$$

where the superscripts are a reminder that these matrices can only be expected to accurately approximate the nonlinear dynamics within a neighborhood of the nominal conditions used for linearization. When designing a linear MPC controller for nonlinear systems, it is common to either i) linearize the system once about the initial condition x_0 or some desired operating condition, or ii) repeatedly linearize the system about the current operating condition x_k at every discrete update of the controller.

2.3 Open-loop Model Comparison

Fig. 2 shows the degree of model error introduced by discretization ($\Delta t = 100$ sec) and linearization. This discretization step size was chosen to be large enough to make the optimization problems in the following sections computationally tractable with 11,700 second prediction horizons while being small enough to capture the key dynamics of the FTMS. The control input used for this model comparison corresponds to the optimized open-loop input trajectory for the dual-tank system determined in [2]. Since the first two states are pure integrators corresponding to the mass of fuel in the tanks, discretization and linearization do not introduce any additional modeling error. As shown in Fig. 2, the discretization of the fuel temperature differential equation introduces zero steady-state modeling error and a small degree of model error during the transients on the order of 0.5 K.

The largest modeling error comes from linearizing the system about the initial condition, x_0. This linearization introduces both transient and steady-state model error on the order of 70 K, as shown in Fig. 2. Clearly, the linearized model is unable to capture neither i) the bilinear coupling between the mass flow rate input and temperature state which affects the steady-state operating condition nor ii) the effects of the time-varying mass of fuel in Tank 1 on the transient fuel temperature behavior.

However, this linearization error can be drastically reduced by repeatedly linearizing the nonlinear dynamics about the current operation condition, x_k, as shown in Fig. 2. This repeated linearization removes any steady-state modeling error and significantly reduces the transient modeling error to roughly 0.2 K.

From these open-loop model comparisons, it becomes clear how short-horizon linear MPC of nonlinear systems can be highly effective when the control objective is regulation about an equilibrium or reference-tracking. The combination of repeated linearization and short prediction horizons ensures that the linear model remains accurate over the MPC prediction horizon. However, the following sections show the limitations of using a linear model for long-horizon predictions.

3 OPEN-LOOP OPTIMIZATION

Unlike many regulation-oriented controllers, the goal for controlling the FTMS is to optimize a long-term energy management plan over the course of the mission. Over this prediction horizon, the mass of fuel in the fuel tanks will change significantly and the control objective is to use the full state and input spaces to maximize the thermal endurance of the aircraft. Without the ability to re-linearize over the long prediction horizon, it is expected that the linearization error might significantly degrade the ability to effectively plan long-term state and input trajectories using a linear MPC controller.

To assess the impact of including nonlinearity in the dynamic system model used for MPC, the following open-loop

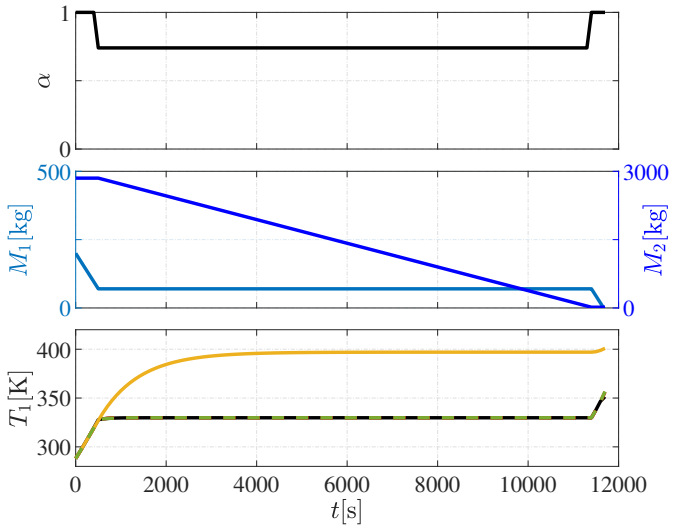

FIGURE 2: Open-loop control input trajectory and corresponding mass and temperature responses. For temperature: continuous nonlinear (black), discrete nonlinear (red, here covered by the green trace line), linear (orange), and successively re-linearized (green).

optimization problem is formulated to maximize thermal endurance:

$$J^*(x_0) = \min_U \sum_{k=0}^{N} \ell(x_k, u_k, s_k), \tag{10a}$$

$$\text{s.t.} \; \forall k \in [0, N-1]$$

$$x_{k+1} = x_k + \Delta t \left[f(x_k, d_k) + g(x_k, d_k) u_k \right], \tag{10b}$$

$$\underline{u} \leq u_k \leq \bar{u}, \tag{10c}$$

$$\underline{x} - s_k \leq x_k \leq \bar{x} + s_k, \tag{10d}$$

$$0 \leq s_k \leq s_{k+1}. \tag{10e}$$

With a prediction horizon of N steps, the input sequence $U = \{u_k\}_{k=0}^{N-1}$ is optimized to minimize the cost function in (10a) designed to maximize thermal endurance and promote smoothness in the input trajectory. For MPC development, minimizing or maximizing the time for task completion is often achieved through the use of binary variables that reflect if the task is completed at each time step [14–16]. The cost function is then formulated to minimize or maximize the sum of these binary variables. However, when including nonlinear dynamics, as in (10b), the introduction of binary variables converts the already hard to solve NLP to a Mixed-Integer Nonlinear Program (MINLP), which is even harder to solve.

Therefore, instead of binary variables, slack variables $s(k)$ are used in (10a), (10d), and (10e) to promote constraint satisfaction and maximize thermal endurance. With thermal endurance defined as the number of discrete time steps before a temperature

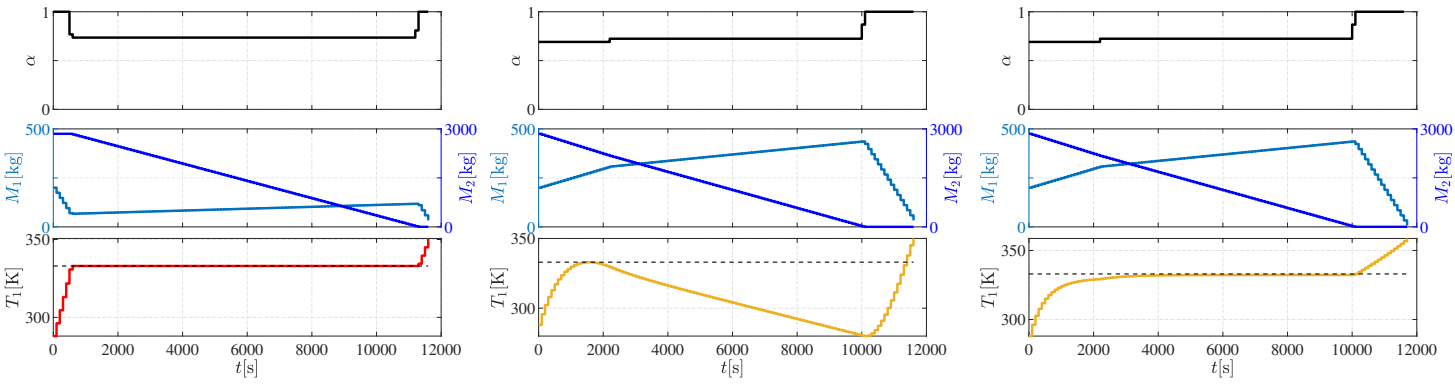

FIGURE 3: Optimized input and state trajectories achieved from solving (10) with (a) nonlinear system dynamics and (b) linear system dynamics (nonlinear model (10b) replaced by the linear model in (9)). In (c), the input trajectory from Fig. 3b is applied to the nonlinear system model in (8).

constraint violation, the cost function (10a) is designed as

$$\ell(x_k, u_k, s_k) = |s_k| + \lambda |u_k - u_{k-1}|, \tag{11}$$

to minimize slack variables and incentivize smooth inputs with $\lambda = 10$. In addition to the nonlinear dynamics constraints (10b), the lower- and upper-bounds on the inputs and states are constrained in (10c) and (10d) based on the limits provided in Table 1. The slack variables are included to maintain feasibility when the fuel temperature exceeds its upper limit while the inequality constraints in (10e) ensure that the slack variables are non-decreasing in time. In combination with (11), (10e) helps to delay the first temperature constraint until as late in the prediction horizon as possible, thus maximizing thermal endurance.

With a discrete-time step size of $\Delta t = 100$ seconds, the prediction horizon is chosen as $N = 117$ steps to capture the $\sim 11{,}600$ seconds constant fuel burn rate example from [2]. All of the results in this paper were generated using MATLAB and YALMIP [17] on a desktop computer with a 3.2 GHz i7-8700 processor and 16 GB of RAM and all nonlinear MPC optimization problems were solved with IPOPT [18] while all linear MPC optimization problems were solved with Gurobi [19]. When solving nonlinear optimization problems, warm-starting the solver with an initial guess at the optimal solution can significantly reduce the computation time. In [2], the author proposes a candidate optimal input trajectory based on the idea of keeping the recirculation tank fuel temperature as high as possible for as long as possible. This is approximately the same trajectory as shown in Fig. 2, and will be used for warm-starting for the following results.

Fig. 3a shows the optimized input and state trajectories based on solving (10) using the nonlinear system model. Note that the applied heat load is held constant at $\dot{Q}_{in} = 109{,}380$ kW, which is slightly higher than the 104,380 kW used in [2] to ensure that the thermal endurance is less than the endurance imposed by the limited mass of fuel. For the first 500 seconds, the optimal input is $\alpha = 1$, which drains fuel from Tank 1 and allows T_1 to quickly rise to the upper-bound $\bar{T} = 333K$. For approximately the next 10,700 seconds, the optimal input is α =0.74, which holds T_1 at steady-state effectively maximizing the amount of energy that is removed from the FTMS via the fuel sent to the engine. Once Tank 2 is almost empty, the control input must return to $\alpha = 1$ to only pull fuel from Tank 1. At this time T_1 is forced to exceed its upper-bound resulting in a thermal endurance of 11,200 seconds. Overall, this optimal open-loop operation is very similar to that determined in [2] resulting in a similar thermal endurance. Note that despite the use of warm-starting with a relatively accurate guess at the input and state trajectories, the computation time to solve (10) is around 123 seconds.

When the nonlinear model in (10b) is replaced with the linear model from (9), the corresponding "optimal" input and state trajectories are shown in Fig. 3b. When comparing the input trajectories in Figs. 3a and 3b, the key difference is that the input no longer starts at $\alpha = 1$ before dropping down to $\alpha = 0.7$. As a result, T_1 in Fig. 3b increases more gradually compared to the rapid increase shown in Fig. 3a. As discussed in [2], maintaining a high value of T_1 increases the temperature of fuel sent to the engine, T_e, and in turn maximizes energy removal from the system with this fuel flow. Solving (10) with the nonlinear model correctly identifies this optimal behavior while solving (10) with the linear model does not. Instead, the linear model predicts a large decrease in temperature which is not physically possible in the nonlinear system. This results in an "expected" thermal endurance of 11,300 seconds, which is even greater than the 11,200 seconds achieved with the nonlinear model.

To demonstrate the risk of using a linear model of the FTMS for long-term trajectory planning, Fig. 3c shows the true state

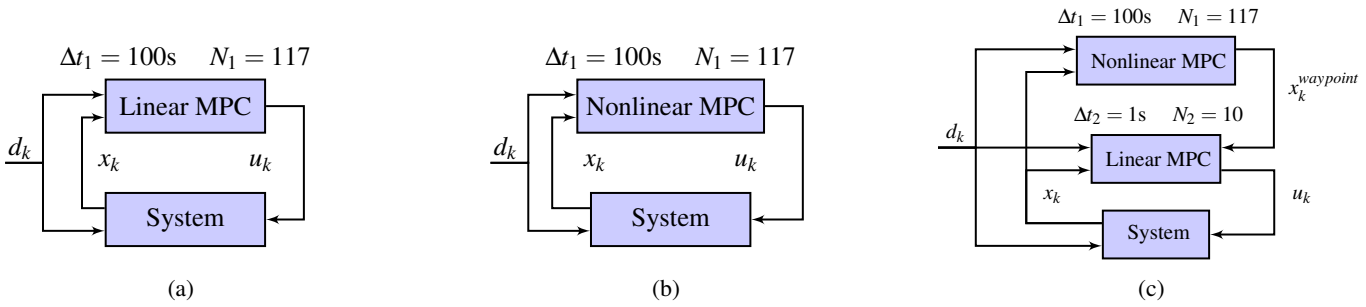

FIGURE 4: Closed-loop control schemes with corresponding sampling time Δt and prediction horizon N: (a) Linear MPC, (b) Nonlinear MPC, and (c) Hierarchical MPC.

trajectory when the "optimal" input from Fig. 3b is applied in open-loop to the nonlinear system. While the fuel mass trajectories are the same, the large decrease in temperature seen in Fig. 3b is no longer seen in Fig. 3c. Instead, T_1 remains close to its upper bound until Tank 2 is empty, at which point the temperature constraint is violated. By using an initial value of $\alpha = 1$ in early operation, optimization using the nonlinear model was able to delay when fuel is drained from Tank 2, which directly delays when Tank 2 is empty and when T_1 violates the temperature constraint. This clearly highlights how early system operation can have a lasting, long-term effect on the system that directly influences the achieved thermal endurance. While optimization using the linear model had predicted a thermal endurance of 11,300 seconds, the achieved thermal endurance using this input trajectory is only 10,100 seconds, which is 9.8% lower than that achieved using the nonlinear model. However, while solving (10) with the nonlinear model required a computation time of 123 seconds, the use of a linear model reduces this computation time to only 0.05 seconds.

4 CLOSED-LOOP MPC

4.1 CONTROL APPROACHES

Instead of applying optimized open-loop control input trajectories directly to the system, MPC is able to compensate for model uncertainty by repeatedly solving (10) at every discrete-time step based on the current state of the system. As an added benefit, when applying linear MPC, the nonlinear dynamics can be re-linearized about the current operating condition, x_k, to generate a more accurate prediction model. Thus, in the remainder of this work, the performance of three MPC schemes is compared, as shown in Fig. 4 with the corresponding sampling times and prediction horizon. For the Linear and Nonlinear MPC the same formulation from the previous section is used. In the Linear MPC the model is re-linearized every time step. The proposed Hierarchical MPC is detailed in Section 4.2.

Since (10) is defined to predict to the end of system operation, (10) is slightly modified to create an MPC controller with a *shrinking* prediction horizon, which is applied to all three controllers. As such, regardless of the current time step, the MPC controllers only predict to the final time step $t_F = 11,700$ seconds and no further. The technical details for formulating an MPC controller with a shrinking horizon are provided in [14].

4.2 HIERARCHICAL MPC

The main contribution of this work is the mixed-linearity hierarchical MPC shown in Fig. 4c. As will be shown in Section 5, a nonlinear model of the FTMS system dynamics is needed to achieve the maximum thermal endurance. However, given the relatively large computation time associated with solving NLPs, a nonlinear MPC formulation is only practical if the update step size Δt can be made large enough to accommodate this solution time. Unfortunately, designing an MPC controller with a large update step size introduces new challenges, especially when the system is subject to unknown disturbances. If a controller cannot react quickly, such disturbances can cause unexpected constraint violations that reduce thermal endurance and negate the benefit of using a nonlinear controller.

Therefore, a mixed-linearity hierarchical MPC formulation serves as an ideal combination of nonlinear and linear MPC that leverages their unique advantages and overcomes their individual limitations. This paper proposes a two-level hierarchy (Fig 4c), with nonlinear MPC at the upper-level and linear MPC at the lower-level. The upper-level controller has the same time step size, $\Delta t_1 = 100$ seconds, as the centralized nonlinear MPC in order to achieve a long prediction horizon with relatively few discrete steps. The lower-level controller has a smaller time step size, $\Delta t_2 = 1$ second, to improve disturbance rejection and the overall responsiveness of the controller. Additionally, the lower-level controller is designed with a shrinking and resetting prediction horizon such that the controller is always predicting to the next update of the upper-level controller. With a prediction horizon of $N_2 = 100$ steps and a time step of $\Delta t_2 = 1$ second, a full nonlinear hierarchy with controllers using nonlinear models at both levels is unlikely to achieve real-time computation given

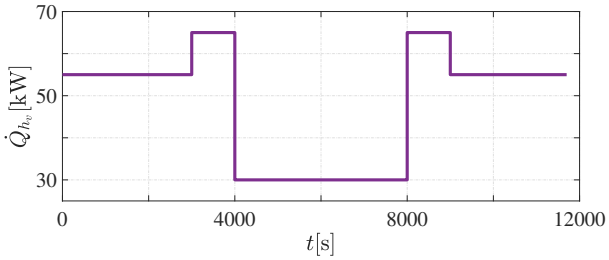

FIGURE 5: Known time-varying heat load disturbance profile.

the computationally demanding task at the lower-level of solving a complex nonlinear optimization problem in 1 second.

To coordinate the decisions made by the two controllers, this paper employs the waypoint-based coordination approach from [14]. This waypoint-based coordination is imposed as a terminal constraint in the lower-level MPC formulation such that the last state in the prediction horizon must exactly equal the optimal state at that time step as determined by the upper-level controller. In this way, the lower-level controller is able to deviate from the upper-level controller's plan between the slow updates Δt_1 to further improve control performance. However, the waypoint constraint provides a simple mechanism to ensure that the short-sighted lower-level controller follows the long-term plan optimized by the upper-level controller to maximize thermal endurance.

In [14], feasibility of this terminal constraint is guaranteed due to the fact that both the upper-level and lower-level controllers are formulated based on the same discrete-time linear model. Unfortunately, the proposed mixed-linearity hierarchical MPC formulation does not benefit from the same guarantee due to linearization error introduced in the model used by the lower-level controller. Therefore, the terminal constraint from [14] is slightly modified to bound the difference between the terminal state of the lower-level controller, x_{k+N}, and the optimal state determined by the upper-level controller, x^*_{k+N}, as

$$-s_{waypoint} \leq x_{k+N} - x^*_{k+N} \leq s_{waypoint}, \tag{12}$$

where $0 \leq s_{waypoint}$ is an additional slack variable that bounds this difference and is penalized with a large weighting term when added to (11).

5 NUMERICAL RESULTS

5.1 Time-varying known disturbance

The performance of the controllers proposed in Section 4 is evaluated under three scenarios: i) with no external disturbances, ii) with known, low-frequency, large disturbances, and finally iii) with unknown, high-frequency, random disturbances. The source of disturbances is considered the parameter $\dot{Q}_{h_v}$. In the first scenario, $\dot{Q}_{h_v}$ is kept constant at its nominal value from Table 1. In the second case, $\dot{Q}_{h_v}$ is designed to deviate from the nominal value as shown in Fig. 5. This profile is provided as preview to the MPC controllers. And in the final scenario, $\dot{Q}_{h_v}$ is randomly perturbed every 10 seconds within the range of 20% to 170% of its nominal value. In this case the controllers only have knowledge of the nominal constant value for trajectory planing. The high-frequency disturbance is considered to be measurable, so the current value of $\dot{Q}_{h_v}$ is fed to the lower-level controller in the Hierarchical MPC. The measured value is not provided to the upper-level controller or the Nonlinear MPC since their update rates are too slow to effectively take advantage of this information. Throughout this section the reader is referred to Table 2 for exact values of computation times and thermal endurance obtained for each case.

TABLE 2: SUMMARY OF CONTROLLER PERFORMANCE.

Scenario	Controller	Thermal Endurance [s]	Computation time[b] [s]	
			Average	Max
Constant Heat Load	Linear	10700	0.02	0.03
	Nonlinear	11207	0.22	2.16
	Hierarchical	11237	0.23/0.026	2.19/0.863
Known disturbances	Linear	8000	0.02	0.06
	Nonlinear	11103	0.42	2.76
	Hierarchical	11106	0.37/0.025	2.38/0.059
Unknown disturbances	Nonlinear	10152	0.24	3.9
	Hierarchical	10706	0.52/0.025	9.5/0.084

[b] Hierarchical MPC: values refer to upper-level/lower-level controllers.

5.2 Constant Heat Load

Figs. 6a and 6b show the closed-loop MPC results based on the nonlinear and linear models, respectively. As expected, the nonlinear closed-loop results are very similar to the open-loop results from Fig. 3a due to the lack of model error, resulting in an achieved thermal endurance of 11,207 seconds. As for the closed-loop Linear MPC results, the input trajectory obtained is similar to the one obtained with the open-loop optimization using the linear model. The resulting thermal endurance is 10,700 seconds, which is 4.5% less than that achieved using the nonlinear controller. This highlights the need for a more accurate model for long-term prediction and thermal endurance maximization, such as the one used by the Nonlinear MPC. As expected though, the sub-optimal performance of the Linear MPC comes with a much lower computational cost as shown in Table 2.

Fig. 6c shows the input and state trajectories of the Hierarchical MPC. Note that the rapid changes in the control input at roughly 11600 seconds occurs after the temperature constraint is violated and has no effect on the thermal endurance. In the absence of time-varying and unknown disturbance, the control performance of the Hierarchical MPC closely resembles that of the Nonlinear MPC controller from Fig. 6a. Thus, the key result for this constant heat load case is demonstrating the effective-

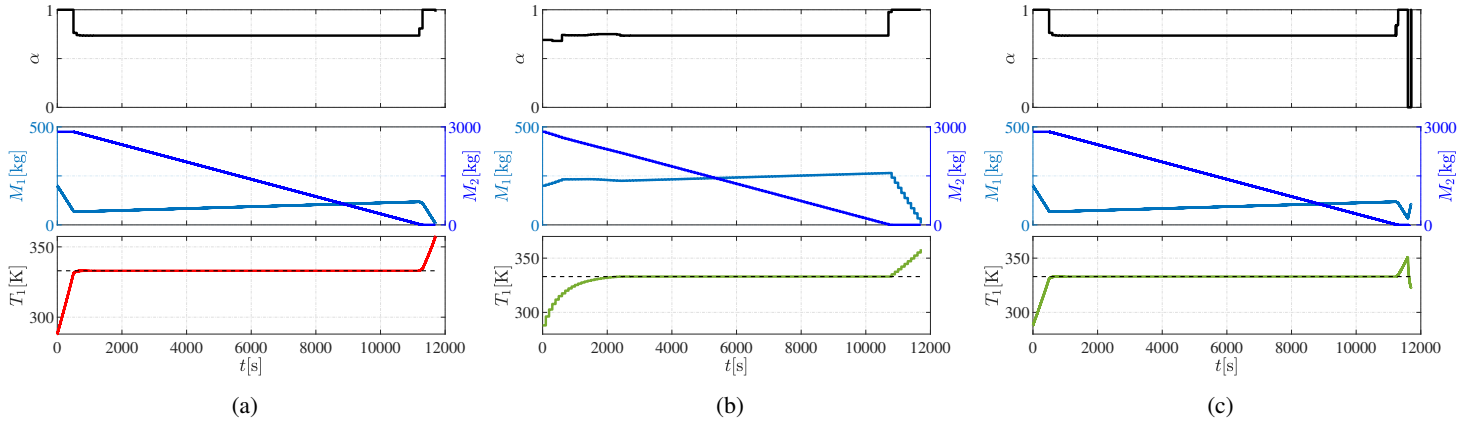

FIGURE 6: Input, mass, and temperature trajectories when using the (a) Nonlinear MPC, (b) Linear MPC (re-linearized at each time step), and (c) Hierarchical MPC controllers in closed-loop with the nonlinear model in (8).

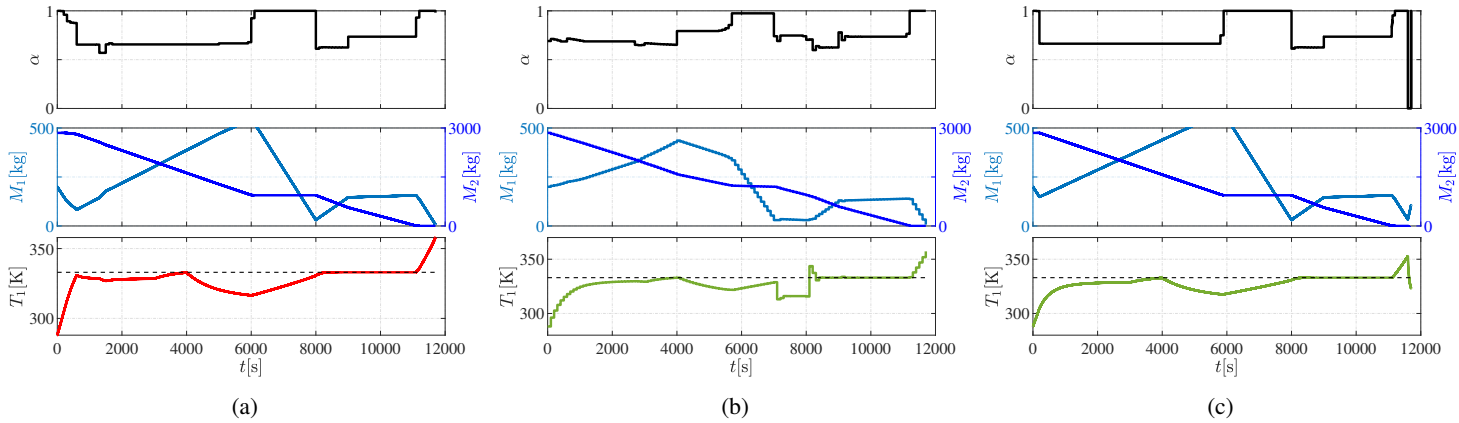

FIGURE 7: Input, mass, and temperature trajectories when using the (a) Nonlinear MPC, (b) Linear MPC, and (c) Hierarchical MPC controllers and subject to the known time-varying disturbance from Fig. 5.

ness of the waypoint coordination between the two controllers of the hierarchy and that the linear lower-level control is able to produce the optimal input trajectory despite the linearization error. Consequently, the state trajectories and the corresponding thermal endurance are also very similar. Considering the computation times obtained, these results show that the use of a linear lower-level controller does not compromise the performance achieved by the Nonlinear MPC while not requiring significant additional computation time.

Fig. 7 shows the closed-loop control results for the Nonlinear, Linear, and Hierarchical MPC controllers under known time-varying disturbances. All three controllers increase α to drain more fuel from Tank 1 when the heat load is decreased in preparation for the second large heat load at 8,000 seconds. However, the Linear MPC (Fig. 7b) does not accurately anticipate the effect of this sudden increase in heat load at 8,000 seconds, resulting in a 10K temperature constraint violation. Therefore, the resulting thermal endurance is only 8,000 seconds. Alternatively, both the Nonlinear MPC and the Hierarchical MPC accurately predict the effects of the time-varying heat load and are capable of executing the transient system operation required to maintain T_1 below its upper-bound. The resulting thermal endurance is 11,103 for the Nonlinear MPC and 11,106 seconds for the Hierarchical MPC. As seen by the approximately 15K of precooling the fuel in Tank 1 between 4,000 and 6,000 seconds, maximizing thermal endurance is no longer as simple as maximizing T_1, as in the constant heat load scenarios from Section 5.2.

5.3 High frequency unknown disturbance

Note that, due to its poor performance on previous simulations, the Linear MPC is not included in the analysis of this section to better focus on the comparison between the Nonlinear MPC and Hierarchical MPC.

As preview of the high-frequency disturbance is not known

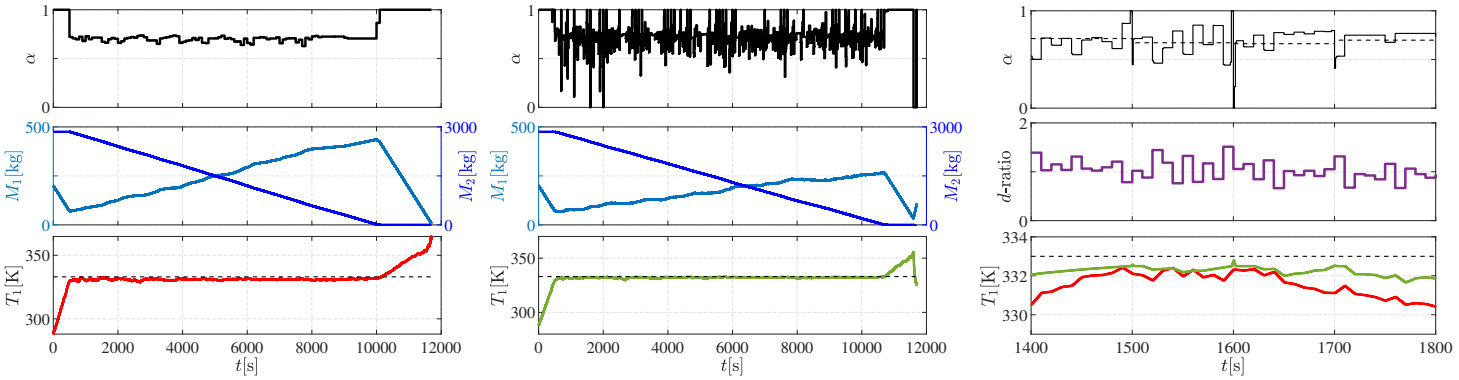

FIGURE 8: Input, mass, and temperature trajectories when using the (a) Nonlinear MPC and (b) Hierarchical MPC controllers and subject to high-frequency unknown disturbances. In (c): detail view of input (Nonlinear MPC dashed; Hierarchical MPC solid), disturbance ratio d-ratio $= \frac{\dot{Q}_{h_v}}{\dot{Q}_{h_v}^{nominal}}$, and temperature (Nonlinear MPC red; Hierarchical MPC green) trajectories for this scenario.

to the controllers, the uncertainly in the closed-loop system is expected to produce temperature constraint violations much earlier than the usual temperature rise at the end of operation. When using the original temperature constraints from Table 1, constraint violations of up to 2K and 0.5K were observed for the Nonlinear MPC and Hierarchical MPC controllers, respectively. The magnitude of these constraint violations is a measure of each controller's disturbance rejection capabilities. Since the objective is to prevent violations of any magnitude, the temperature constraint for each controller is tightened by the amount necessary to prevent premature violations of the original constraints. Therefore, the temperature constraint is reduced by 2K for the Nonlinear MPC and 0.5K for the Hierarchical MPC.

Fig. 8 shows the response obtained with the constraint tightening for both controllers, including a 400 second view of the simulations where the effect of the high-frequency disturbance can be better seen. With the constraint tightening, both controllers were capable of keeping the temperature below the original constraint value.

Compared to the closed-loop control under a constant heat load (Sections 4 and 4.2), the Hierarchical MPC had a reduction in thermal endurance of 531 seconds while the Nonlinear MPC had a reduction of 1,055 seconds. These results not only show how the unknown disturbances affect thermal endurance but also highlight the differences in disturbance rejection capabilities of both controllers. By tightening the temperature constraint to accommodate for the disturbances, the average fuel temperature in the recirculation tank is effectively being lowered, thereby reducing the amount of heat that is rejected to the engine and consequently reducing the thermal endurance. The more the constraint is reduced, the lower the thermal endurance. Fig. 8c shows an important feature of the MPC-based lower-level controller where the input is able to increase and decrease very rapidly around 1600 seconds to prevent a constraint violation while still tracking the desired long-term fuel mass and temperature trajectories provided by the upper-level controller in the form of a waypoint. This aggressive, multi-objective behavior could not be easily achieved by replacing the lower-level controller by a static feedback control law.

Thus, a key benefit of the Hierarchical MPC when compared to the Nonlinear MPC is the inclusion of the lower-level MPC controller that provides superior disturbance rejection resulting in less stringent constraint tightening needed to ensure safe operation.

6 CONCLUSION

A mixed-linearity hierarchical MPC formulation was presented to maximize the thermal endurance of aircraft by accounting for nonlinear dynamics in the Fuel Thermal Management System. Model linearization techniques typically used for MPC of nonlinear systems were shown to produce large modeling errors over long-term prediction horizons, resulting in a 5-10% reduction in thermal endurance compared to optimized trajectories using a nonlinear model. With a nonlinear model in the upper-level and a linear model in the lower-level, the mixed-linearity hierarchical MPC controller was shown to be a computationally efficient and effective approach that benefits from capturing system nonlinearities over long prediction horizons and fast update rates for improved disturbance rejection. Future work will focus on quantifying linearization error and computationally-efficient methods for nonlinear reachability analysis to develop a robust hierarchical MPC framework for the control of nonlinear systems with guaranteed constraint satisfaction.

ACKNOWLEDGMENT

This material is based upon work supported by the National Science Foundation under Grant No. 1849500.

REFERENCES

[1] Henson, M. A., 1998. "Nonlinear model predictive control: current status and future directions". *Computers & Chemical Engineering,* ***23***, 12, pp. 187–202.

[2] Doman, D. B., 2018. "Fuel Flow Topology and Control for Extending Aircraft Thermal Endurance". *Journal of Thermophysics and Heat Transfer,* ***32***(1), pp. 35–50.

[3] Lui, C., Carrillo Arce, E., Banks, C., Ho, B., Walia, P., Lee, C., Canto, G., Iden, S., and Maldonado, M., 2010. "Potential Technology to Unclog Hot Day Operational Limit". *SAE Power Systems Conference*.

[4] Ganev, E., and Koerner, M., 2013. "Power and Thermal Management for Future Aircraft". *SAE AeroTech Congress & Exhibition*.

[5] Doty, J., Yerkes, K., Byrd, L., Murthy, J., Alleyne, A., Wolff, M., Heister, S., and Fisher, T. S., 2017. "Dynamic Thermal Management for Aerospace Technology: Review and Outlook". *Journal of Thermophysics and Heat Transfer,* ***31***(1).

[6] Bodie, M., Russell, G., Mccarthy, K., Lucus, E., Zumberge, J., and Wolff, M., 2010. "Thermal Analysis of an Integrated Aircraft Model". *48th AIAA Aerospace Sciences Meeting*.

[7] Roberts, R. A., and Eastbourn, S. M., 2014. "Vehicle Level Tip-to-Tail Modeling of an Aircraft". *International Journal of Thermodynamics,* ***17***(2).

[8] Jain, N., and Hencey, B. M., 2016. "Increasing fuel thermal management system capability via objective function design". *American Control Conference*, pp. 549–556.

[9] Pangborn, H. C., Hey, J. E., Deppen, T. O., Alleyne, A. G., and Fisher, T. S., 2017. "Hardware-in-the-Loop Validation of Advanced Fuel Thermal Management Control". *Journal of Thermophysics and Heat Transfer,* ***31***(4).

[10] Pangborn, H. C., Koeln, J. P., Williams, M. A., and Alleyne, A. G., 2018. "Experimental Validation of Graph-Based Hierarchical Control for Thermal Management". *Journal of Dynamic Systems, Measurement, and Control,* ***140***.

[11] Jasa, J. P., Mader, C. A., and Martins, J. R., 2018. "Trajectory optimization of a supersonic aircraft with a thermal fuel management system". *AIAA Multidisciplinary Analysis and Optimization Conference*.

[12] Koeln, J. P., Pangborn, H. C., Williams, M. A., Kawamura, M. L., and Alleyne, A. G., 2019. "Hierarchical Control of Aircraft Electro-Thermal Systems". *IEEE Transactions on Control Systems Technology*.

[13] Huang, G. P., Doman, D. B., Rothenberger, M. J., Hencey, B., DeSimio, M. P., Tipton, A., and Sigthorsson, D. O., 2019. "Dimensional Analysis, Modeling, and Experimental Validation of an Aircraft Fuel Thermal Management System". *Journal of Thermophysics and Heat Transfer,* ***33***(4).

[14] Koeln, J. P., and Alleyne, A. G., 2018. "Two-Level Hierarchical Mission-Based Model Predictive Control". *American Control Conference*.

[15] Richards, A., and How, J. P., 2003. "Model predictive control of vehicle maneuvers with guaranteed completion time and robust feasibility". *American Control Conference*.

[16] Richards, A., and How, J. P., 2006. "Robust variable horizon model predictive control for vehicle maneuvering". *International Journal of Robust and Nonlinear Control,* ***16***(7), pp. 333–351.

[17] Lofberg, J., 2004. "YALMIP: a toolbox for modeling and optimization in MATLAB". *2004 IEEE International Conference on Computer Aided Control Systems Design*.

[18] Kawajir, Y., Laird, C. D., and Waechter, A., 2010. "Introduction to IPOPT: A tutorial for downloading, installing, and using IPOPT .".

[19] Gurobi Optimization, L. L. C., 2016. Gurobi Optimizer Reference Manual.